STRUCTURAL SCIENCE
CRYSTAL ENGINEERING
MATERIALS

Volume 73 (2017)

Supporting information for article:

Nature of E2X2 σ(4c–6e) of the X---E–E---X type at naphthalene 1,8-positions and model, elucidated by X-ray crystallographic analysis and QC calculations with QTAIM approach

Yutaka Tsubomoto, Satoko Hayashi, Waro Nakanishi, Takahiro Sasamori and Norihiro Tokitoh

Electronic Supplementary Information

Nature of E_2X_2 σ(4c–6e) of the X---E–E---X type at naphthalene 1,8-positions and model, elucidated by X-ray crystallographic analysis and QC calculations with QTAIM approach

Yutaka Tsubomoto,[a] Satoko Hayashi,[a,*] Waro Nakanishi,[a,*] Takahiro Sasamori,[b] and Norihiro Tokitoh[b]

[a] *Department of Material Science and Chemistry, Faculty of Systems Engineering, Wakayama University, 930 Sakaedani, Wakayama, 640-8510 Japan*
E-mail: nakanisi@sys.wakayama-u.ac.jp and hayashi3@sys.wakayama-u.ac.jp
[b] *Institute for Chemical Research, Kyoto University, Gokasho, Uji, Kyoto, 611-0011, Japan*

QTAIM Dual Functional Analysis (QTAIM-DFA)

The bond critical point (BCP; ∗) is an important concept in QTAIM. The BCP of (ω, σ) = (3, –1) (Bader, 1990; Matta, 2007) is a point along the bond path (BP) at the interatomic surface, where charge density $\rho(\boldsymbol{r})$ reaches a minimum. It is donated by $\rho_b(\boldsymbol{r}_c)$. While the chemical bonds or interactions between A and B are denoted by A–B, which correspond to BPs between A and B in QTAIM, A-∗-B emphasizes the presence of BCP (∗) in A–B.

The sign of the Laplacian $\rho_b(\boldsymbol{r}_c)$ ($\nabla^2\rho_b(\boldsymbol{r}_c)$) indicates that $\rho_b(\boldsymbol{r}_c)$ is depleted or concentrated with respect to its surrounding, since $\nabla^2\rho_b(\boldsymbol{r}_c)$ is the second derivative of $\rho_b(\boldsymbol{r}_c)$. $\rho_b(\boldsymbol{r}_c)$ is locally depleted relative to the average distribution around $\boldsymbol{r}_c$ if $\nabla^2\rho_b(\boldsymbol{r}_c) > 0$, but it is concentrated when $\nabla^2\rho_b(\boldsymbol{r}_c) < 0$. Total electron energy densities at BCPs ($H_b(\boldsymbol{r}_c)$) must be a more appropriate measure for weak interactions on the energy basis (Bader, 1990; Matta, 2007; Bader, 1985, 1990, 1991, 1998; Bader et al., 1983; Matta, & Boyd, 2007; Biegler-König & Schönbohm, 2002; Biegler-König et al., 1982, 2001; Tang et al., 1985; Nakanishi et al., 2007, 2008b, 2009, 2012; Nakanishi & Hayashi, 2010a, 2010b). $H_b(\boldsymbol{r}_c)$ are the sum of kinetic energy densities ($G_b(\boldsymbol{r}_c)$) and potential energy densities ($V_b(\boldsymbol{r}_c)$) at BCPs, as shown in Equation (S1). Electrons at BCPs are stabilized when $H_b(\boldsymbol{r}_c) < 0$, therefore, interactions exhibit the covalent nature in this region, whereas they exhibit no covalency if $H_b(\boldsymbol{r}_c) > 0$, due to the destabilization of electrons at BCPs under the conditions (Bader, 1990; Matta, 2007). Equation (S2) represents the relation between $\nabla^2\rho_b(\boldsymbol{r}_c)$ and $H_b(\boldsymbol{r}_c)$, together with $G_b(\boldsymbol{r}_c)$ and $V_b(\boldsymbol{r}_c)$, which is closely related to the virial theorem.

$$H_b(\boldsymbol{r}_c) = G_b(\boldsymbol{r}_c) + V_b(\boldsymbol{r}_c) \quad \text{(S1)}$$

$$(\hbar^2/8m)\nabla^2\rho_b(\boldsymbol{r}_c) = H_b(\boldsymbol{r}_c) - V_b(\boldsymbol{r}_c)/2 \quad \text{(S2)}$$

$$= G_b(\boldsymbol{r}_c) + V_b(\boldsymbol{r}_c)/2 \quad \text{(S2')}$$

Interactions are classified by the signs of $\nabla^2\rho_b(\boldsymbol{r}_c)$ and $H_b(\boldsymbol{r}_c)$. Interactions in the region of $\nabla^2\rho_b(\boldsymbol{r}_c) < 0$ are called shared-shell (SS) interactions and they are closed-shell (CS) interactions for $\nabla^2\rho_b(\boldsymbol{r}_c) > 0$. $H_b(\boldsymbol{r}_c)$ must be negative when $\nabla^2\rho_b(\boldsymbol{r}_c) < 0$, since $H_b(\boldsymbol{r}_c)$ are larger than $(\hbar^2/8m)\nabla^2\rho_b(\boldsymbol{r}_c)$ by $V_b(\boldsymbol{r}_c)/2$ with negative $V_b(\boldsymbol{r}_c)$ at all BCPs (Equation (S2)). Consequently, $\nabla^2\rho_b(\boldsymbol{r}_c) < 0$ and $H_b(\boldsymbol{r}_c) < 0$ for the SS interactions. The CS interactions are especially called *pure* CS interactions for $H_b(\boldsymbol{r}_c) > 0$ and $\nabla^2\rho_b(\boldsymbol{r}_c) > 0$, since electrons at BCPs are depleted and destabilized under the conditions (Bader, 1990). Electrons in the intermediate

region between SS and *pure* CS, which belong to CS, are locally depleted but stabilized at BCPs, since $\nabla^2\rho_b(\boldsymbol{r}_c) > 0$ but $H_b(\boldsymbol{r}_c) < 0$ (Bader, 1990). We call the interactions in this region *regular* CS (Nakanishi et al., 2008b, 2009; Nakanishi & Hayashi, 2010a), when it is necessary to distinguish from *pure* CS. The role of $\nabla^2\rho_b(\boldsymbol{r}_c)$ in the classification can be replaced by $H_b(\boldsymbol{r}_c) - V_b(\boldsymbol{r}_c)/2$, since $(\hbar^2/8m)\nabla^2\rho_b(\boldsymbol{r}_c) = H_b(\boldsymbol{r}_c) - V_b(\boldsymbol{r}_c)/2$ (Equation (S2)).

We proposed QTAIM-DFA by plotting $H_b(\boldsymbol{r}_c)$ versus $H_b(\boldsymbol{r}_c) - V_b(\boldsymbol{r}_c)/2$ (= $(\hbar^2/8m)\nabla^2\rho_b(\boldsymbol{r}_c)$) (Nakanishi et al., 2009), after the proposal of $H_b(\boldsymbol{r}_c)$ versus $\nabla^2\rho_b(\boldsymbol{r}_c)$ (Nakanishi et al., 2008b). Both axes in the plot of the former are given in energy unit, therefore, distances on the (x, y) (= $(H_b(\boldsymbol{r}_c) - V_b(\boldsymbol{r}_c)/2, H_b(\boldsymbol{r}_c))$ plane can be expressed in the energy unit, which provides an analytical development. QTAIM-DFA can incorporate the classification of interactions by the signs of $\nabla^2\rho_b(\boldsymbol{r}_c)$ and $H_b(\boldsymbol{r}_c)$. Scheme S1 summarizes the QTAIM-DFA treatment. Interactions of *pure* CS appear in the first quadrant, those of *regular* CS in the forth quadrant and SS interactions do in the third quadrant. No interactions appear in the second one.

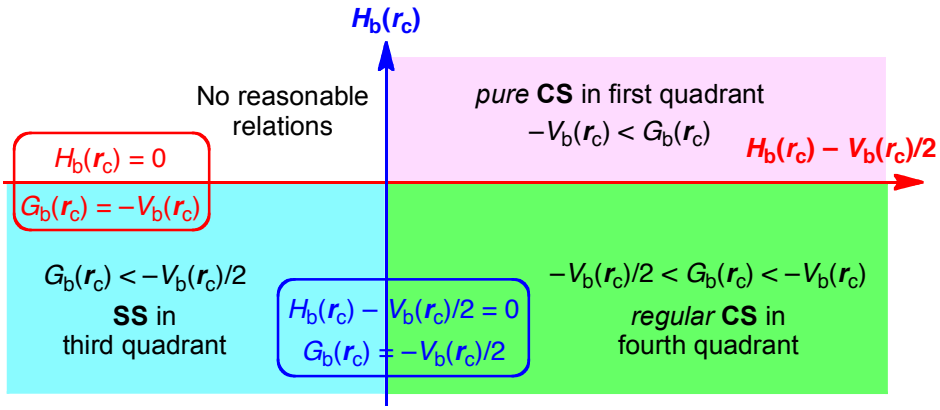

Scheme S1. QTAIM-DFA: Plot of $H_b(\boldsymbol{r}_c)$ versus $H_b(\boldsymbol{r}_c) - V_b(\boldsymbol{r}_c)/2$ for Weak to Strong Interactions

In our treatment, data for perturbed structures around fully optimized structures are also employed for the plots, together with the fully optimized ones (see Fig. S1) (Nakanishi et al., 2008b, 2009, 2012; Nakanishi & Hayashi, 2010a, 2010b). We proposed the concept of the "dynamic nature of interaction" originated from the perturbed structures. The behavior of interactions at the fully optimized structures corresponds to "the static nature of interactions", whereas that containing perturbed structures exhibit the "dynamic nature of interaction" as explained below. The method to generate the perturbed structures is discussed later. Plots of $H_b(\boldsymbol{r}_c)$ versus $H_b(\boldsymbol{r}_c) - V_b(\boldsymbol{r}_c)/2$ are analyzed employing the polar coordinate (R, θ) representation with (θ_p, κ_p) parameters (Nakanishi et al., 2009, 2012; Nakanishi & Hayashi, 2010a, 2010b). Fig. S1 explains the treatment. R in (R, θ) is defined by Equation (S3) and given in the energy unit. R corresponds to the energy for an interaction at BCP. The plots show a spiral stream, as a whole. θ in (R, θ) defined by Equation (S4), measured from the y-axis, controls the spiral stream of the plot. Each plot for an interaction shows a specific curve, which provides important information of the interaction (see Fig. S1). The curve is expressed by θ_p and κ_p. While θ_p, defined by Equation (S5) and measured from the y-direction, corresponds to the tangent line of a plot, where θ_p is calculated employing data of the perturbed structures with a fully-optimized structure and κ_p is the curvature of the plot (Equation (S6)). While (R, θ) correspond to the static nature, (θ_p, κ_p) represent the dynamic nature of interactions. We call (R, θ) and (θ_p, κ_p) QTAIM-DFA parameters, whereas $\rho_b(\boldsymbol{r}_c)$, $\nabla^2\rho_b(\boldsymbol{r}_c)$, $G_b(\boldsymbol{r}_c)$, $V_b(\boldsymbol{r}_c)$, $H_b(\boldsymbol{r}_c)$ and $H_b(\boldsymbol{r}_c)$ –

$V_b(\boldsymbol{r}_c)/2$ belong to QTAIM functions. $k_b(\boldsymbol{r}_c)$, defined by Equation (S7), is an QTAIM function but it will be treated as if it were an QTAIM-DFA parameter, if suitable.

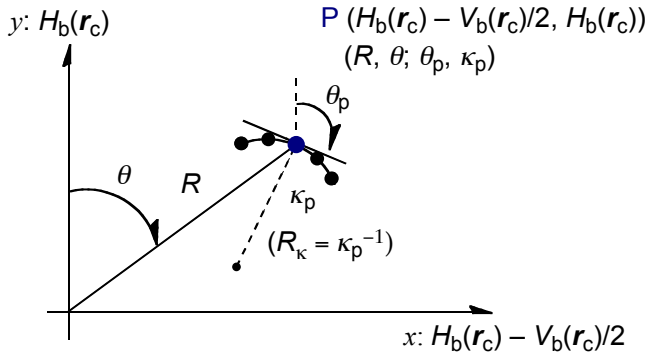

Figure S1. Polar (R, θ) coordinate representation of $H_b(\boldsymbol{r}_c)$ versus $H_b(\boldsymbol{r}_c) - V_b(\boldsymbol{r}_c)/2$, with ($\theta_p$, κ_p) parameters.

$$R = (x^2 + y^2)^{1/2} \quad \text{(S3)}$$

$$\theta = 90^\circ - \tan^{-1}(y/x) \quad \text{(S4)}$$

$$\theta_p = 90^\circ - \tan^{-1}(dy/dx) \quad \text{(S5)}$$

$$\kappa_p = |d^2y/dx^2| / [1 + (dy/dx)^2]^{3/2} \quad \text{(S6)}$$

$$k_b(\boldsymbol{r}_c) = V_b(\boldsymbol{r}_c)/G_b(\boldsymbol{r}_c) \quad \text{(S7)}$$

where $(x, y) = (H_b(\boldsymbol{r}_c) - V_b(\boldsymbol{r}_c)/2, H_b(\boldsymbol{r}_c))$

Criteria for Classification of Interactions: Behavior of Typical Interactions Elucidated by QTAIM-DFA

$H_b(\boldsymbol{r}_c)$ are plotted versus $H_b(\boldsymbol{r}_c) - V_b(\boldsymbol{r}_c)/2$ for typical interactions in vdW (van der Waals interactions), HB (hydrogen bonds), CT-MC (molecular complexes through charge transfer), X_3^- (trihalide ions), CT-TBP (trigonal bipyramidal adducts through charge-transfer), Cov-w (weak covalent bonds) and Cov-s (strong covalent bonds) (Nakanishi et al., 2008b, 2009, 2012; Nakanishi & Hayashi, 2010a, 2010b). Rough criteria are obtained, after the analysis of the plots for the typical interactions according to Equations (S3)–(S7), by applying QTAIM-DFA. Scheme S2 shows the rough criteria, which are accomplished by the θ and θ_p values, together with the values of $k_b(\boldsymbol{r}_c)$. The criteria will be employed to discuss the nature of interactions in question, as a reference.

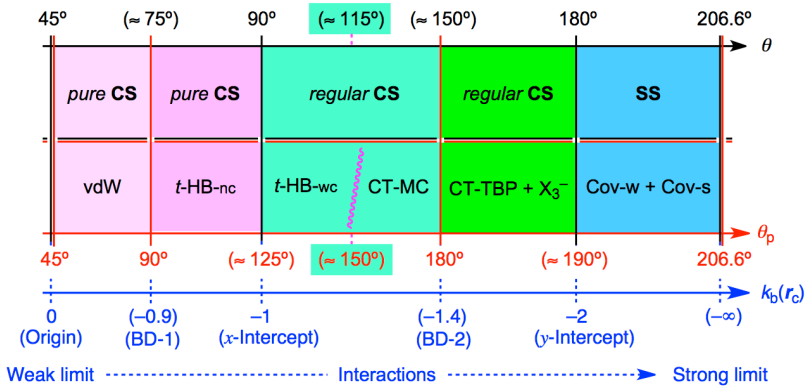

Scheme S2. Rough classification of interactions by θ and θ_p, together with $k_b(\boldsymbol{r}_c)$ (= $V_b(\boldsymbol{r}_c)/G_b(\boldsymbol{r}_c)$).

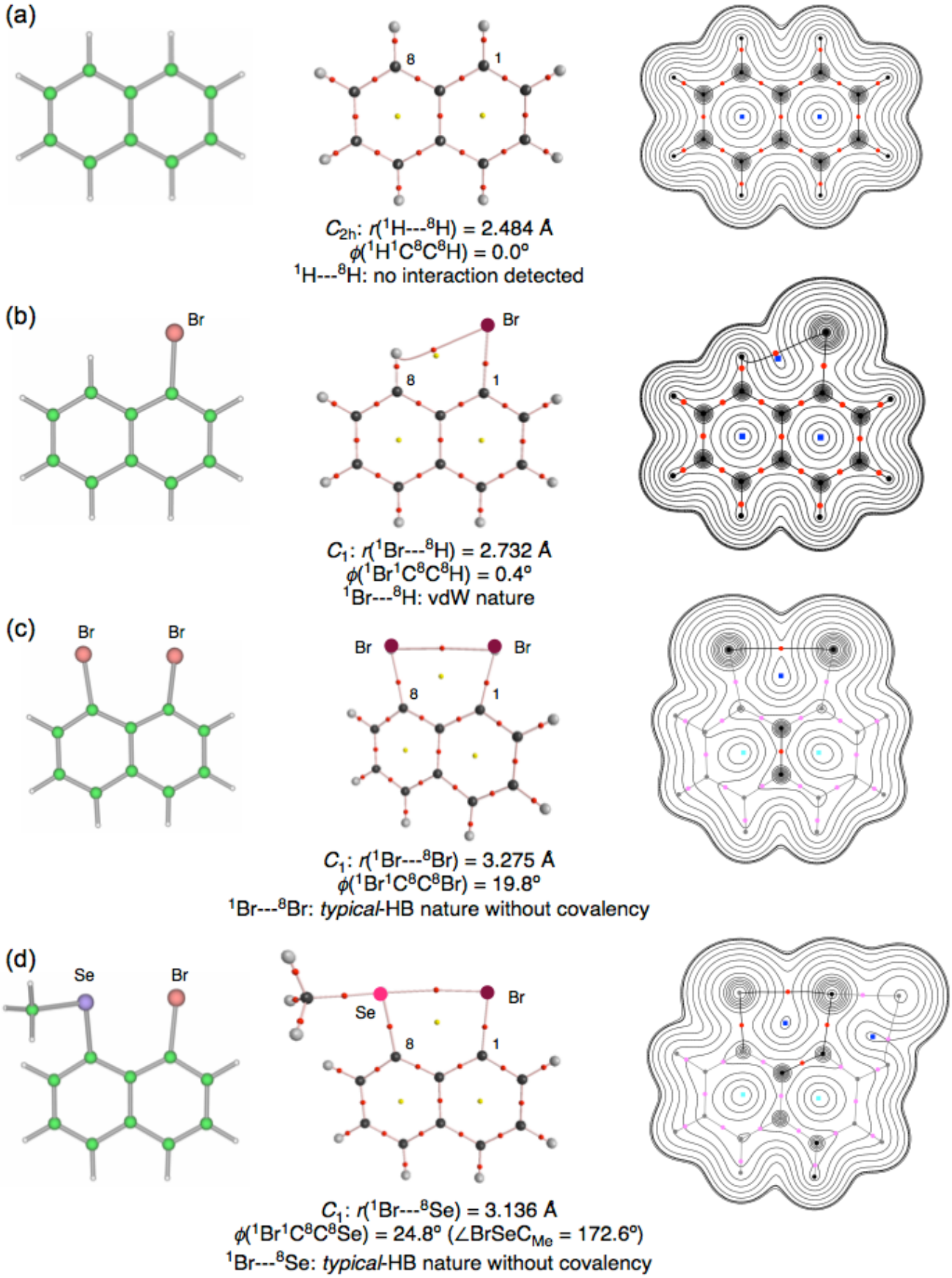

Figure S2. Molecular graphs and contour plots of $\rho_b(\boldsymbol{r}_c)$ on the optimized structures of $C_{10}H_8$ and 1-Br-8-$YC_{10}H_6$ (Y = H, Br, and SeMe) with MP2/BSS-A. Colors and marks are the same as those in Fig. 4 in the text.

Table S1. QTAIM functions and parameters for ^{1}H-∗-^{8}Y, ^{1}X-∗-^{8}Y, and ^{1}X-∗-^{8}Se at BCPs of 1-Br-8-YC$_{10}$H$_6$ (Y = H, Br, and SeMe) and 1-Cl-8-YC$_{10}$H$_6$ (Y = SeMe), optimized with MP2/BSS-A.[(a)]

Compd (^{1}X-^{8}Y)[(b)]	$\rho_b(\boldsymbol{r}_c)$ (ea_o^{-3})	$c\nabla^2\rho_b(\boldsymbol{r}_c)$[(c)] (au)	$H_b(\boldsymbol{r}_c)$ (au)	$k_b(\boldsymbol{r}_c)$[(d)]	R (au)	θ (º)	Freq[(e)] (cm^{-1})	k_f[(f)] (g)	θ_p (º)	κ_p (au^{-1})
HBr (H-∗-Br)	0.0129	0.0061	0.0019	-0.811	0.0064	72.4	176.8	0.160	–	–
Br_2 (Br-∗-Br)	0.0168	0.0066	0.0011	-0.907	0.0067	80.4	143.4	0.763	100.4	95.4
ClSeMe (Se-∗-Cl)	0.0279	0.0081	-0.0017	-1.095	0.0083	101.9	130.2	0.126	151.4	107
ClSeMe (Se-∗-C)	0.1165	0.0013	-0.0612	-1.960	0.0612	178.8	400.6	3.189	182.6	0.7
BrSeMe (Se-∗-Br)	0.0198	0.0070	0.0004	-0.971	0.0070	86.8	134.3	0.161	121.0	170
BrSeMe (Se-∗-C)	0.1490	-0.0186	-0.0918	-2.681	0.0937	191.5	620.4	1.121	191.3	1.1

(a) The 6-311+G(3df) basis set being employed for S and Se with the 6-311G(d) basis set for C and H; (b) C_1 symmetry; (c) $c\nabla^2\rho_b(\boldsymbol{r}_c) = H_b(\boldsymbol{r}_c) - V_b(\boldsymbol{r}_c)/2$, where $c = \hbar^2/8m$; (d) $k_b(\boldsymbol{r}_c) = V_b(\boldsymbol{r}_c)/G_b(\boldsymbol{r}_c)$; (e) Corresponding to the interaction in question. Symmetric and anti-symmetric modes being employed for ^{A}E-∗-^{A}E and ^{A}E-∗-^{B}E, respectively; (f) Force constant for ν; (g) mdyn Å^{-1}.

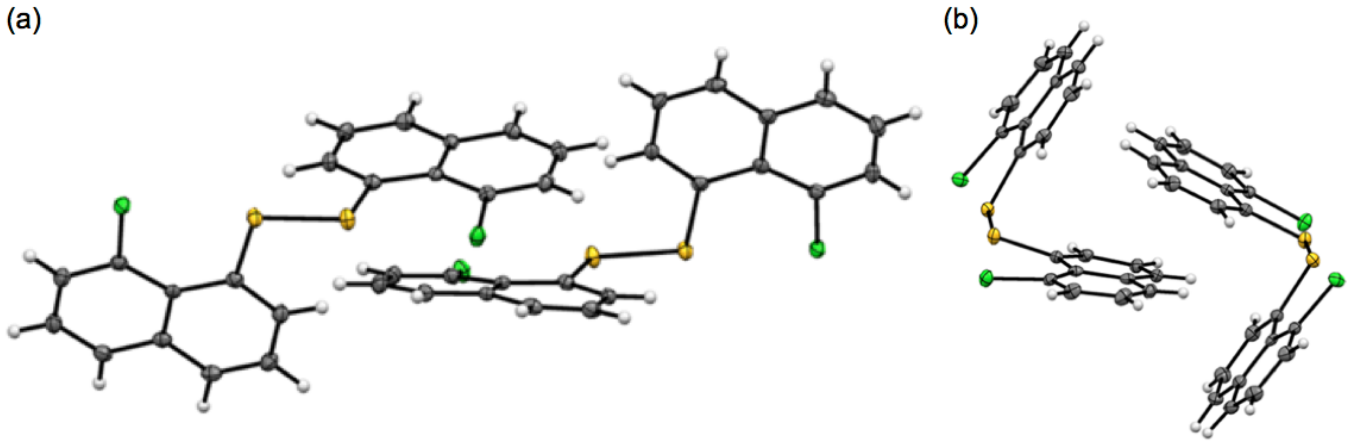

Figure S3. Structure of **1**, determined by the X-ray crystallographic analysis. Thermal ellipsoids are drawn at 50% probability.

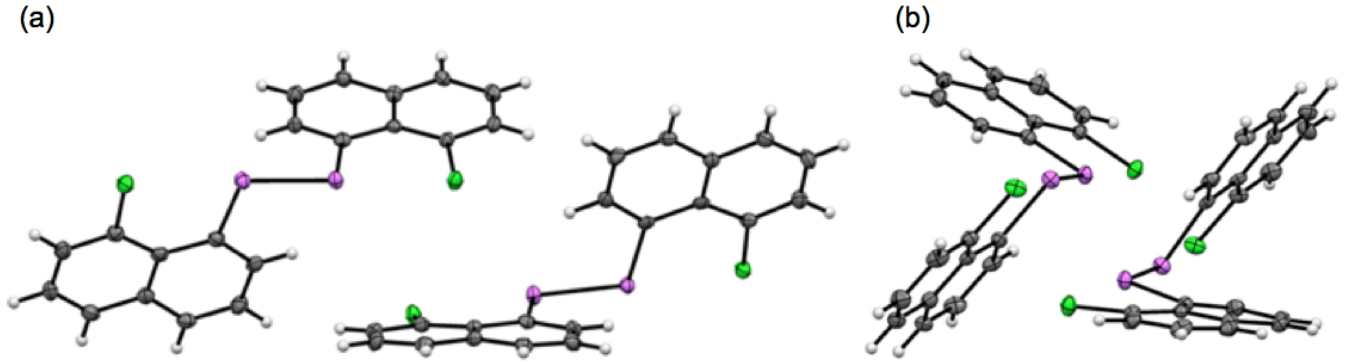

Figure S4. Structure of **3**, determined by the X-ray crystallographic analysis. Thermal ellipsoids are drawn at 50% probability.

Table S2. Crystallographic data for **1**, **3**, and **4**

	1	**3**	**4**
Empirical formula	$C_{20}H_{12}Cl_2S_2$	$C_{20}H_{12}Cl_2Se_2$	$C_{20}H_{12}Br_2Se_2$
Formula weight	387.32	481.12	570.04
Temperature (K)	103(2)	103(2)	103(2)
Crystal system	orthorhombic	orthorhombic	Triclinic
Space group	$Pca2_1$ (#29)	$Pca2_1$ (#29)	P-1 (#2)
Unit cell dimensions			
a (Å)	7.824(2)	7.89330(10)	7.83940(10)
b (Å)	28.782(8)	29.1713(4)	8.0986(2)
c (Å)	14.350(4)	14.4594(2)	15.0650(4)
α (deg)	90.00	90.00	90.9410(10)
β (deg)	90.00	90.00	101.8880(10)
γ (deg)	90.00	90.00	111.0930(10)
Volume (Å^3)	3231.7(15)	3329.39(8)	868.92(3)
Z	8	8	2
Dcalcd (g cm^{-3})	1.592	1.920	2.179
F(000)	1584	1872	540
Reflections observed [I > 2σ(I)]	5988	6129	3813
Parameters	529	433	217
R_1 [I > 2σ(I)]	0.020	0.024	0.0391
R_1 [all data]	0.020	0.026	0.0432
ωR_2 [I > 2σ(I)]	0.052	0.059	0.0788
ωR_2 [all data]	0.052	0.060	0.0805
Goodness-of-fit on F^2	1.073	1.058	1.198

Table S3. Structural parameters evaluated for model **A** [(S, Cl), (S, Br), (Se, Cl), (Se, Br)] (C_2) with MP2/BSS-C.[(a)]

Species	r_o(E, E) (Å)	r_o(E, X) (Å)	Δr_o(E, X)[(b)] (Å)	$\angle H^AE^{A'}E$ (º)	$\angle {}^BX^AE^{A'}E$ (º)	ϕ_1[(c)] (º)	ϕ_2[(d)] (º)	ΔE_{ES} (kJ mol^{-1})	ΔE_{ZP} (kJ mol^{-1})
(S, Cl)	2.0559	3.3838	–0.1662	98.9	170.4	–101.8	–113.2	–26.5	–22.2
(S, Br)	2.0572	3.4947	–0.1533	98.8	171.3	–106.1	–121.7	–26.7	–22.6
(Se, Cl)	2.3220	3.4617	–0.1883	96.7	161.4	–130.2	–169.6	–26.9	–23.6
(Se, Br)	2.3242	3.5805	–0.1695	96.6	160.9	–135.6	179.6	–27.6	–24.3

(a) BSS-C: the 6-311+G(3df) basis sets being employed for S and Se with the 6-311G(d,p) basis sets for C and H; (b) $\Delta r_o({}^AE, {}^BX) = r_o({}^AE, {}^BX) - \Sigma r_{vdW}({}^AE, {}^BX)$, where r_{vdW}(S) = 1.80 Å, r_{vdW}(Se) = 1.90 Å, r_{vdW}(Cl) = 1.75 Å, and r_{vdW}(Br) = 1.85 Å, (Bondi, 1964); (c) $\phi_1 = \phi(H^AE^{A'}EH)$; (d) $\phi_2 = \phi(H^AE^BXMe)$.

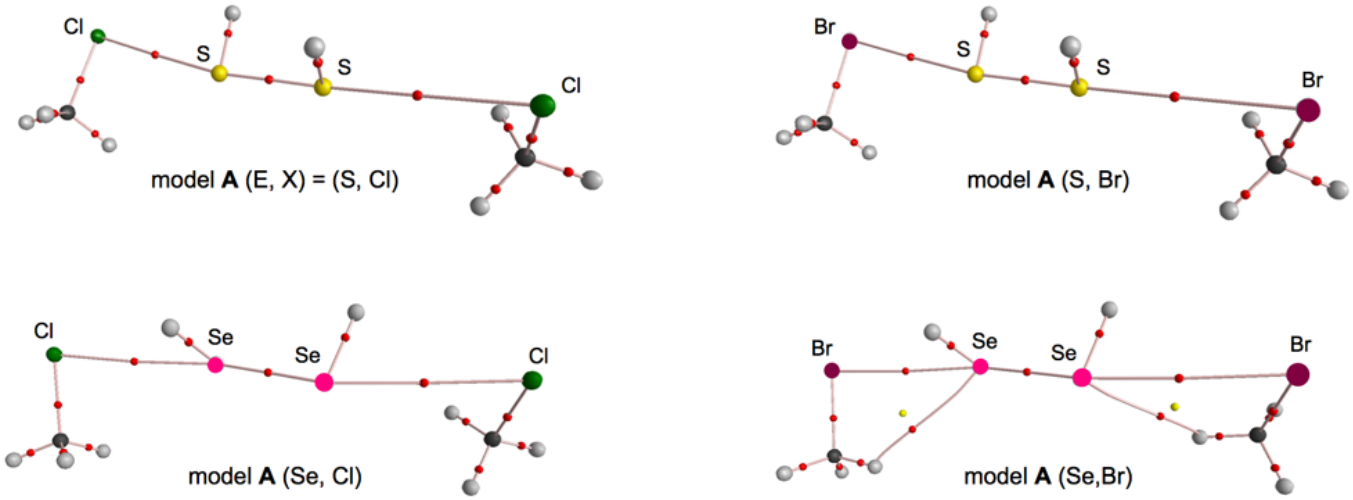

Figure S5. Molecular graphs for models **A** [(E, X) = (S, Cl), (S, Br), (Se, Cl), (Se, Br)]. BCPs (bond critical points) are denoted by red dots, RCPs (ring critical points) by yellow dots, CCPs (cage critical points) by green dots, and BPs (bond paths) by pink lines. Carbon atoms are in black, hydrogen atoms are in gray, and selenium atoms in pink.

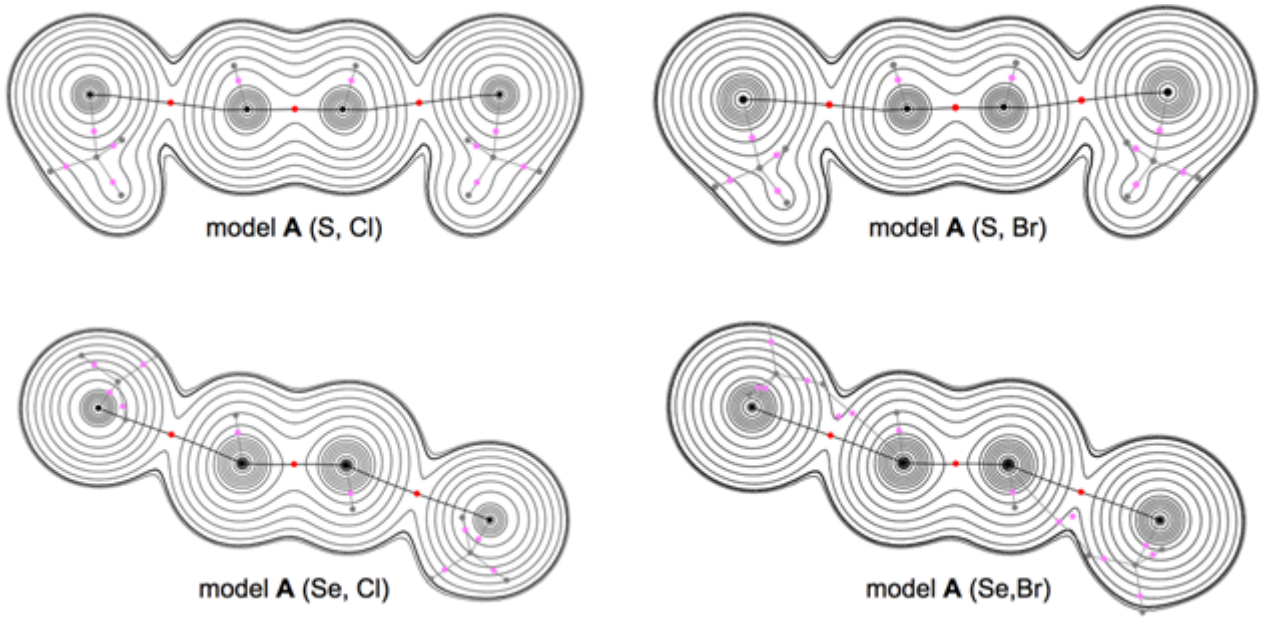

Figure S6. Contour plots of $\rho_b(\boldsymbol{r}_c)$ for models **A** [(E, X) = (S, Cl), (S, Br), (Se, Cl), (Se, Br)]. BCPs on the plane are shown by red dots, those outside of the plane in dark pink dots, RCPs on and outside the plane by blue squares and light blue ones, respectively. CCPs by green squares, and BPs on the plane by black lines and those outside of the plane are by gray lines. Atoms on and outside the plane are by black dots and gray ones, respectively. The contours ($e a_0^{-3}$) are at 2^l ($l = \pm 8, \pm 7, ..., 0$) with 0.0047 (heavy line).

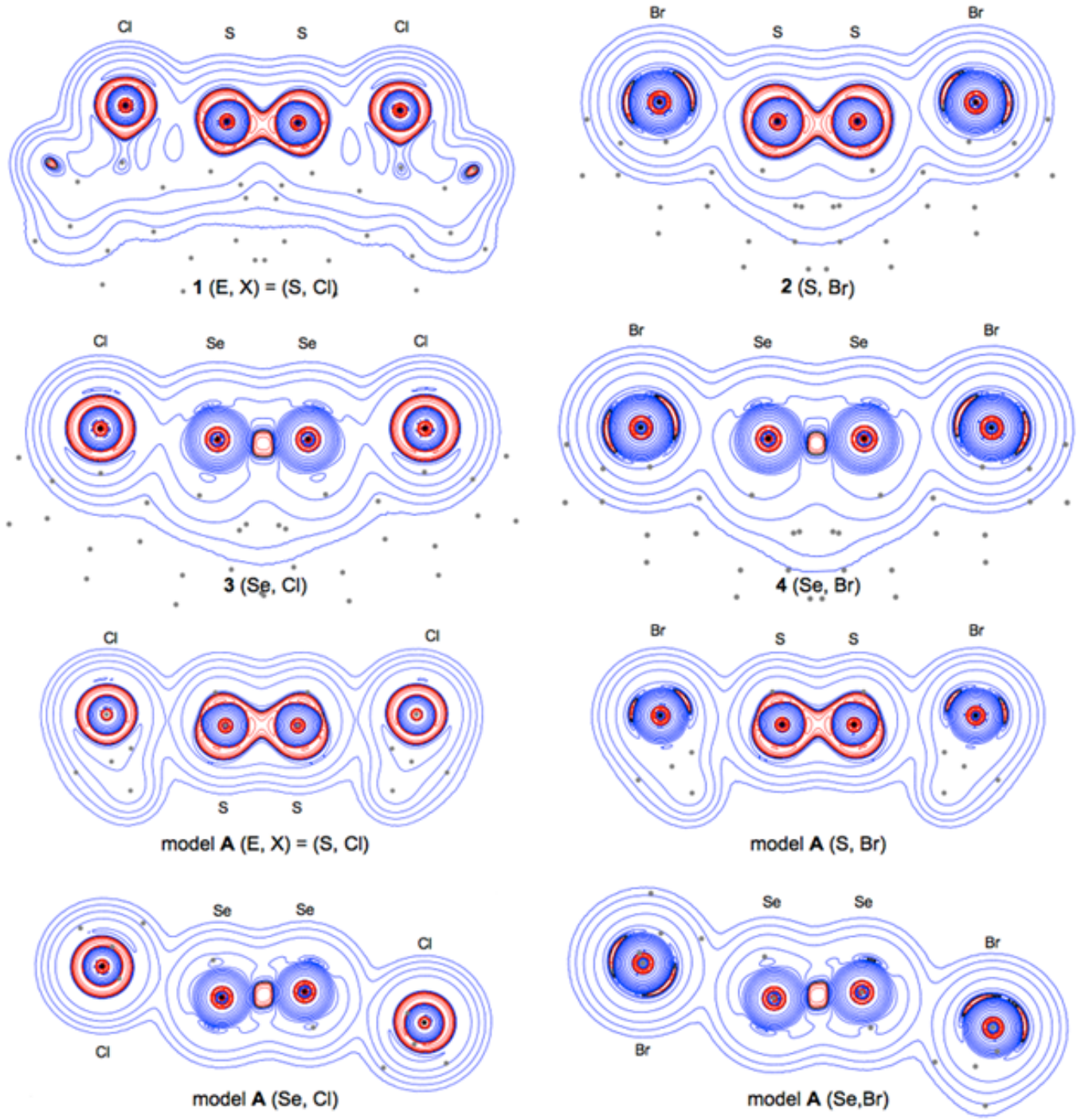

Figure S7. Negative Laplacians for **1**–**4** drawn with M06-2X/BSS-A//MP2/BSS-A and model **A** (S, Cl)–(Se, Br) drawn with MP2/BSS-C//MP2/BSS-C, similarly to the case of Fig. 4 in the text. Blue and red lines correspond to the positive and negative values, respectively.

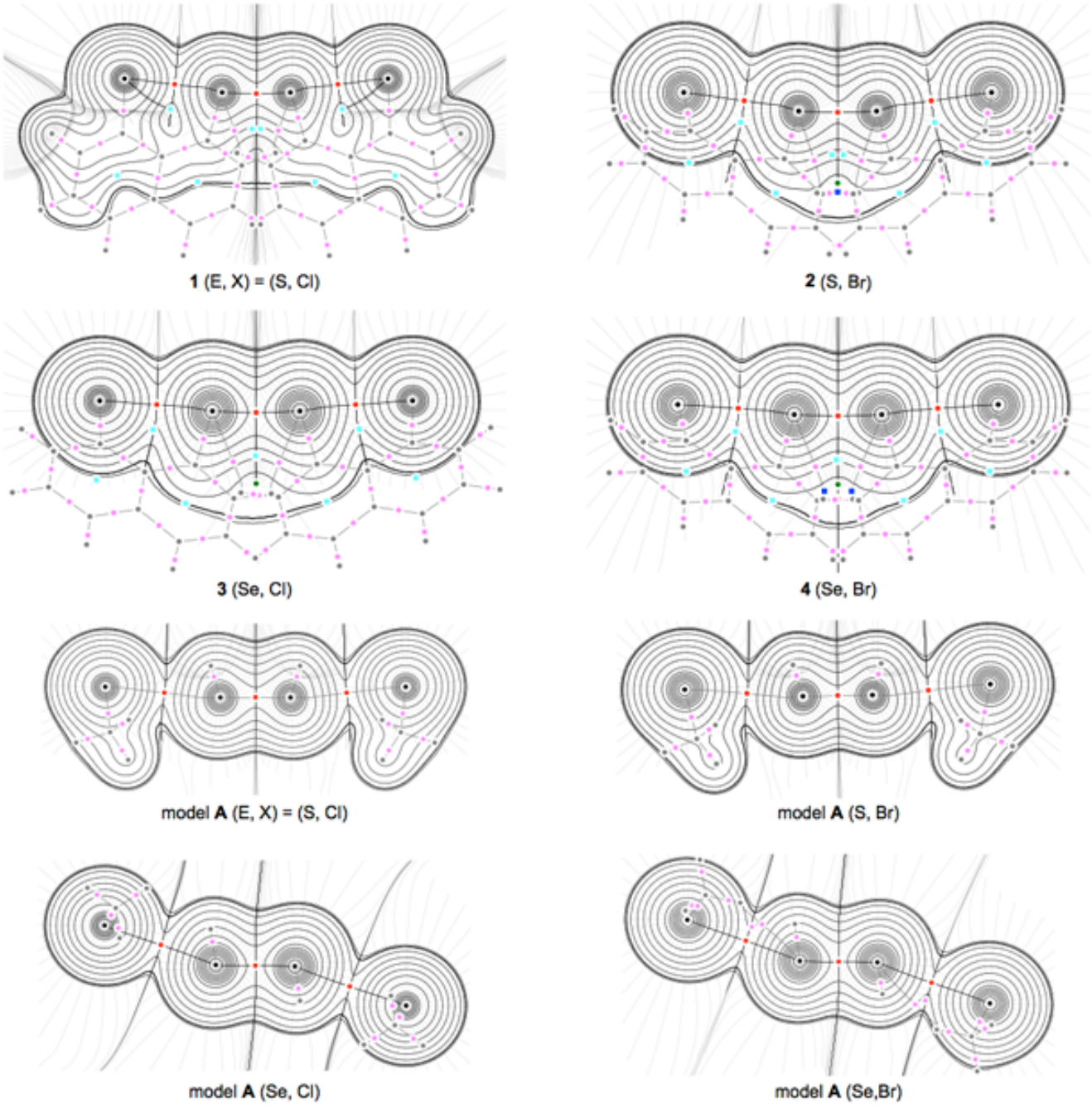

Figure S8. Trajectory plots for **1**–**4** drawn with M06-2X/BSS-A//MP2/BSS-A and model **A** (S, Cl)–(Se, Br) drawn with MP2/BSS-C//MP2/BSS-C, similarly to the case of Fig. 4 in the text. Colors and marks are the same as those in Fig. 4.

Table S4. Results of NBO analysis for the ^{1}E---^{8}X interactions in **1**–**4** with M06-2X/BSS-A//MP2/BSS-A and models **A** [(S, Cl), (S, Br), (Se, Cl), and (Se, Br)] with MP2/BSS-C//MP2/BSS-C.

Compound (^{1}E, ^{8}X)	$E(2)^{(a,b)}$ ([e])	$E(2)^{(a,b)}$ ([f])	$[E(i) - E(j)]^{(c)}$ (au)	$F(i,j)^{(d)}$ (au)	Compound (^{1}E, ^{8}X)	$E(2)^{(a,b)}$ ([e])	$E(2)^{(a,b)}$ ([f])	$[E(i) - E(j)]^{(c)}$ (au)	$F(i,j)^{(d)}$ (au)
calculated									
1 (S, Cl) (C_2)	4.61	19.3	0.51	0.043	**2** (S, Br) (C_2)	4.42	18.5	0.48	0.041
3 (Se, Cl) (C_2)	6.72	28.1	0.47	0.050	**4** (Se, Br) (C_2)	6.66	27.9	0.42	0.047
observed									
1 (S, Cl)$^{(g)}$	4.88$^{(h)}$	20.4$^{(h)}$	0.51$^{(h)}$	0.044$^{(h)}$					
3 (Se, Cl)$^{(g)}$	7.04$^{(h)}$	29.4$^{(h)}$	0.46$^{[h]}$	0.051$^{(h)}$	**4** (Se, Br)	8.59$^{(h)}$	35.9$^{(h)}$	0.42$^{(h)}$	0.054$^{(h)}$
model **A**									
(S, Cl) (C_2)	1.64	6.9	0.49	0.025	(S, Br) (C_2)	1.88	7.9	0.46	0.026
(Se, Cl) (C_2)	2.22	9.3	0.43	0.028	(Se, Br) (C_2)	2.67	11.2	0.40	0.029

(a) Second-order perturbation energy; (b) Only one side of energy is shown; (c) Donor orbital of NBO(i) is n_p(^{8}X or ^{B}X) and acceptor orbital of NBO (j) corresponds to σ*(^{1}E–$^{1'}$E or ^{A}E–$^{A'}$E); (d) Fock matrix; (e) In kcal mol^{-1}; (f) In kJ mol^{-1}; (g) The crystals contain two independent molecules in a unit cell; (h) Averaged value.

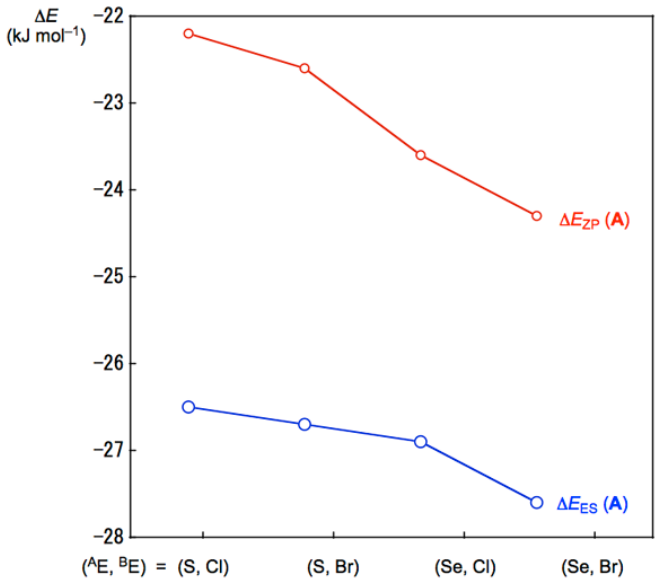

Figure S9. Plot of ΔE_{ES} and ΔE_{ZP} for model **A**.

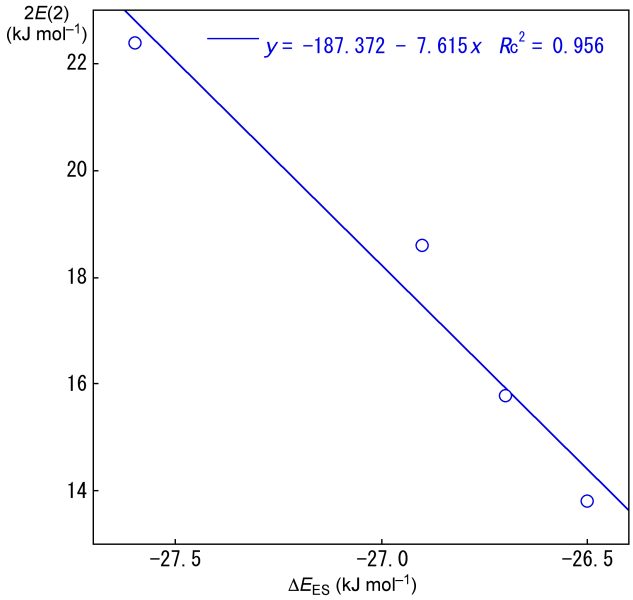

Figure S10. Plot of $2E(2)$ versus ΔE_{ES} for model **A**.

Table S5. r_{BP} and R_{SL} values for the ^{B}X---^{A}E–^{A}E---^{B}X interactions in compounds **1**–**4** with MP2/BSS-A and model **A** with MP2/BSS-C.[a]

Species ^{B}X---^{A}E–^{A}E---^{B}X	R_{SL}(^{8}X, ^{1}E) (Å)	R_{SL}(^{1}E, $^{1'}$E) (Å)	r_{BP}(^{8}X, ^{1}E) (Å)	r_{BP}(^{1}E, $^{1'}$E) (Å)	Δr_{BP}(^{8}X, ^{1}E)[b] (Å)	Δr_{BP}(^{1}E, $^{1'}$E)[c] (Å)
Compounds **1**–**4**						
^{8}Cl-∗-^{1}S-∗-$^{1'}$S-∗-$^{8'}$Cl in **1**	2.9340	2.0311	2.9481	2.0324	0.0142	0.0013
^{8}Br-∗-^{1}S-∗-$^{1'}$S-∗-$^{8'}$Br in **2**	3.0392	2.0330	3.0526	2.0344	0.0134	0.0015
^{8}Cl-∗-^{1}Se-∗-$^{1'}$Se-∗-$^{8'}$Cl in **3**	2.9774	2.3010	2.9824	2.3024	0.0050	0.0014
^{8}Br-∗-^{1}Se-∗-$^{1'}$Se-∗-$^{8'}$Br in **4**	3.0837	2.3072	3.0887	2.3085	0.0050	0.0013
Observed						
^{8}Cl-∗-^{1}S-∗-$^{1'}$S-∗-$^{8'}$Cl in **1**	2.9493	2.0461	2.9630	2.0474	0.0138	0.0013
^{8}Cl-∗-^{1}Se-∗-$^{1'}$Se-∗-$^{8'}$Cl in **3**	2.9708	2.3249	2.9754	2.3264	0.0046	0.0015
^{8}Br-∗-^{1}Se-∗-$^{1'}$Se-∗-$^{8'}$Br in **4**	3.0740	2.3354	3.0791	2.3369	0.0051	0.0015
model **A**						
^{B}Cl-∗-^{A}S-∗-$^{A'}$S-∗-$^{B'}$Cl	3.3838	2.0559	3.3943	2.0576	0.0105	0.0017
^{B}Br-∗-^{A}S-∗-$^{A'}$S-∗-$^{B'}$Br	3.4947	2.0572	3.5052	2.0589	0.0105	0.0017
^{B}Cl-∗-^{A}Se-∗-$^{A'}$Se-∗-$^{B'}$Cl	3.4617	2.3220	3.4682	2.3226	0.0065	0.0006
^{B}Br-∗-^{A}Se-∗-$^{A'}$Se-∗-$^{B'}$Br	3.5805	2.3242	3.5871	2.3248	0.0066	0.0006

(a) BSS-A: the 6-311+G(3df) basis sets being employed for S and Se with the 6-311G(d) basis sets for C and H. BSS-C: the 6-311+G(3df) basis sets being employed for S and Se with the 6-311G(d,p) basis sets for C and H; (b) $\Delta r_{BP}(^{8}X, ^{1}E) = r_{BP}(^{8}X, ^{1}E) - R_{SL}(^{8}X, ^{1}E)$; (c) $\Delta r_{BP}(^{1}E, ^{1'}E) = r_{BP}(^{1}E, ^{1'}E) - R_{SL}(^{1}E, ^{1'}E)$.

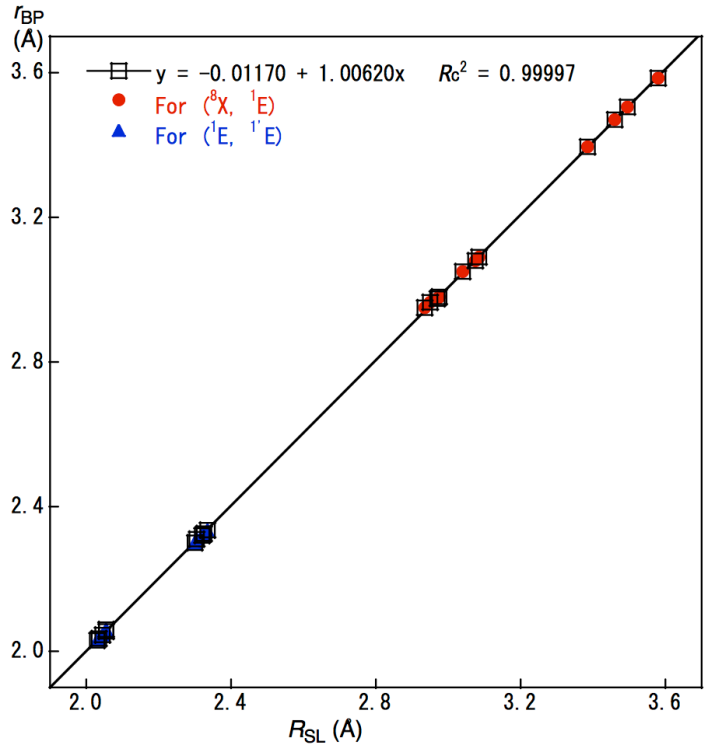

Figure S11. Plots of r_{BP} versus R_{SL} for the interactions in Compounds **1**–**4** and models **A**. Correlation is very good, which are shown in the figure.